



ORIGINAL ARTICLE

Chitosan-Linseed mucilage polyelectrolyte complex nanoparticles of Methotrexate: *In vitro* cytotoxic efficacy and toxicological studies



Shazia Akram Ghumman^{a,*}, Arshad Mahmood^{b,c}, Sobia Noreen^d, Asma Aslam^a,
Bushra Ijaz^e, Amina Amanat^a, Rizwana Kausar^f, Mavra Rana^a, Huma Hameed^{g,h,*}

^a College of Pharmacy, University of Sargodha, Sargodha 40100, Pakistan

^b College of Pharmacy, Al Ain University, Abu Dhabi Campus, Abu Dhabi, United Arab Emirates

^c AAU Health and Biomedical Research Centre (HBRC), Al Ain University, United Arab Emirates

^d Institute of Chemistry, University of Sargodha, Sargodha 40100, Pakistan

^e Centre of Excellence in Molecular Biology (CEMB), University of the Punjab, Lahore 53700, Pakistan

^f ILM College of Pharmaceutical Sciences, Sargodha 40100, Pakistan

^g Univ Rennes, Inserm, EHESP, IRSET-UMR_S 1085, Rennes, France

^h Faculty of Pharmacy, University of Central Punjab, Lahore-54000, Pakistan

Received 22 July 2022; accepted 21 November 2022

Available online 25 November 2022

KEYWORDS

Linseed mucilage;
Methotrexate;
Polyelectrolyte complex;
Sustained release;
In vivo cytotoxicity;
Antitumor effects

Abstract The goal of this research was to develop, fabricate and analyze polymeric nanoparticles for the administration of methotrexate (MTX). Linseed mucilage and chitosan nanoparticles (NPs) were prepared using a slightly modified polyelectrolyte complex (PEC) method. The size, shape, and encapsulation effectiveness of the resultant nanoparticles were measured. MTX release profiles at gastrointestinal pH (1.2 and 7.4) and tumor pH (5.5) were examined to determine the targeted potential of NPs as pH-responsive nanocarriers. Zeta analysis showed that nanoparticles prepared by PEC have a size range of 192.1 nm to 246 nm, and PDI was 0.3 of the optimized formulation, which showed homogenous nature of prepared nanoparticles formulation. The findings demonstrated that NPs have a low polydispersity index and a positive zeta potential (PDI). The *in-vitro* release of the drug indicated a pH-dependent, sustained drug release up to 24 h. Blank LSMCSNPs had almost no *in-vivo* cytotoxicity for 14 days, while optimum MTX loaded NPs had strong anti-tumor effects on HepG2 and MCF-7 cells as measured by the MTT assay. Cell apoptosis induction was also checked and MCF-7 cells treated with MTX-LSMCSNPs had a significantly greater rate of

* Corresponding authors.

E-mail addresses: shazia.akram@uos.edu.pk (S. Akram Ghumman), huma.hameed@ucp.edu.pk (H. Hameed).

Peer review under responsibility of King Saud University.



apoptosis (21.2 %) than those treated with MTX alone (14.14 %). The findings show that LSMCSNPs could be a potential delivery mechanism for methotrexate to cancer cells in a secure, steady, and ideally controlled manner to improve therapeutic outcomes.

© 2022 The Author(s). Published by Elsevier B.V. on behalf of King Saud University. This is an open access article under the CC BY license (<http://creativecommons.org/licenses/by/4.0/>).

1. Introduction

Chemotherapy has been used as the most common first-line cancer treatment. Many chemotherapy drugs have poor water solubility and their efficacy was challenged because cancer cells can develop resistance. Methotrexate (MTX) is commonly used to treat a variety of cancers as a solely or in combination with the anti-cancer medications including brain cancer, primary central nervous system, carcinoma and leptomeningeal metastatic cancer (Rahimi et al., 2017). However, because of its poor solubility, inadequate targeting impairs its therapeutic effectiveness, leading to side effects such as alopecia, nausea, body pains, hepatotoxicity and myelosuppression; hence the use of MTX is restricted, causing patients' anticancer treatments to be disrupted (Zhao et al., 2016). Nanoparticles, as chemotherapy drugs, provide effective interventions (e.g., nanostructured lipid carriers, biopolymers and synthetic nanostructures, micro emulsion, dendrimers, and carbon nanofibers) for trying to target cancerous cells and lesion zones without having caused major harm to normal tissues (Jia et al., 2014).

The emphasis on nanotechnology investigation had shifted during the last era towards smarter biopolymers, polysaccharide, and lipids. Polymeric nanoparticles (PNPs) have the capacity to achieve a constant carrier delivery by modifying their formula for the intended effect, particularly in conjunction to their nanometer dimensions (De Jong and Borm 2008). Polysaccharides have been considered as potential anti-tumor treatments. Several polysaccharides were used to treat cancers therapeutically or adjuvant, they not only reduce the risks but also helped to achieve sufficient therapeutic parameters with minimal side effects (Li et al., 2021).

Linseeds mucilage (LSM) commonly known as alsiflaxseed has been commonly utilized as a food stuff, LSM is anionic in nature, and belongs to the family *Liniaceae* (Elleuch et al., 2011). Upon soaking in hot water, linseeds released mucilage that was primarily made of Arabinoxylans (1470 kDa) and Rhamnogalacturonan (high molecular weight fraction, (1510 kDa) and low molecular weight fraction, (341 kDa)). Prospective structure of LSM; suggested as RG-I bridge-linked arabinans is shown in Fig. 1 (Naran et al., 2008, Qian et al., 2012, Liu et al., 2018, Sheikh et al., 2020).

Polysaccharides in linseed mucilage have swelling (pH-dependent), swelling-de-swelling ability in response to stimuli, silver reduction, and capping capability (Haseeb et al., 2016, Haseeb et al., 2017). The low cost and dynamic properties of linseed mucilage motivate researchers to employ it as a green polymer in new medication delivery (Nasrabadi et al., 2019). Chitosan (CS) is a cationic polymer produced by the deacetylation of alkaline chitin. From food processing to targeted cellular payload delivery, it has a wide range of medicinal applications. Because of its cationic nature, CS is often used in NPs, which helps to reduce circulation time and increase

bioavailability when exposed to biological conditions (Kwak et al., 2019).

Several methods of chitosan NPs production have been proposed, including (i) ionic gelation (Lima et al., 2012), (ii) coacervation (Dash et al., 2011) (iii) liquid diffusion (Chiesa et al., 2018) (iv) spray-drying technique (Antoniraj et al., 2020) (v) solvent evaporation (Liu et al., 2011), and (vi) polyelectrolyte complexation (Ciro et al., 2020). Because of their easy processability and lack of organic solvents, polyelectrolyte complex formation and ionic gelation method are the most extensively employed procedures for the production of NP frameworks (Salem et al., 2019). Saffron delivery nanocarriers based on CS-gum Arabic polyelectrolyte bioactive chemicals; nanocapsules with a diameter of 193 nm were created in a spherical form (Rajabi et al., 2019). When oppositely charged macromolecules interact, polyelectrolyte complexes formed. PECs are a kind of association complex created by molecules with opposing charges, such as drug polymer, polymer-polymer, or polymer-drug-polymer (Patwekar et al., 2016, Potaš et al., 2020).

The goal of this research was to formulate and characterize MTX-LSMCSNPs using linseed mucilage and chitosan using polyelectrolyte complex method. The size, shape, and encapsulation effectiveness of the resultant nanoparticles were all measured. To verify the target efficacy of NPs as pH-responsive nanoparticles, the release rate of MTX was studied at gastrointestinal pH (1.2 and 7.4) and tumor pH (5.5). We further evaluated the survivability of HepG2 and MCF-7 cells as well as non-cancerous cells, with MTX-LSMCSNPs, indicating that MTX-LSMCSNPs might have been a viable alternative to the existing anticancer medications with fewer side effects.

2. Experimental

2.1. Materials

Methotrexate was received as a gift from Rotex Pharma Pvt. Ltd. Pakistan and linseeds were purchased from the local market of Sargodha, Pakistan. Sigma-Aldrich, Germany provided Chitosan (Medium; 75–85 % de-acetylated). Analytical grade Glacial acetic acid (Sigma-Aldrich, Germany), Dimethyl Formamide (DMFA) (Sigma-Aldrich, Germany), 37 % HCL, Ethanol (Sigma-Aldrich, Germany) were used. Dialysis membrane (Sigma-Aldrich, Germany). All procedures were conducted utilizing deionized water.

2.2. Extraction of mucilage (LSM) from linseed

LSM was obtained from ripe and matured Linseeds by immersing 200 g of linseeds in 1000 mL of distilled water at 37 °C for 4 h. Thereafter, we heated these immersed linseeds in electrical water bath until the slurry was formed. Further, refrigeration of this linseed slurry was done for a couple of

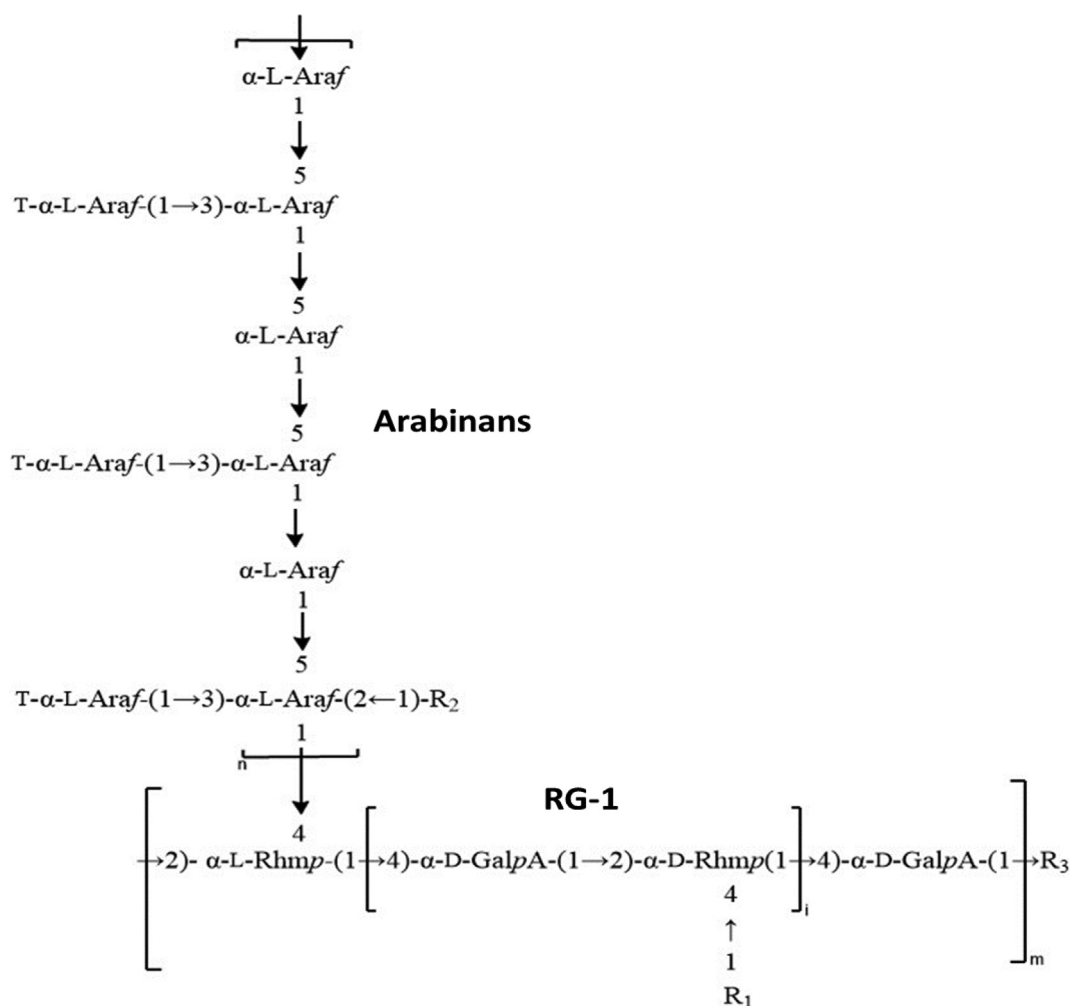


Fig. 1 Possible structure of LSM; proposed as RG-1 bridge-linked Arabinans.

hours until the undissolved material settled down. The filtered slurry was precipitated using ethyl alcohol. The formed precipitates were placed in a petri dish to dry up to for 24 h. After drying into hard, tough crystals, they were grounded by using a pestle and mortar, then sieved by sieve # 80 and stored in the desiccators for further use (Moghaddas et al., 2019).

2.3. Physicochemical properties of LSM

The amount (%) of gel content, solubility behavior, and pH of extracted LSM were done according to B.P guidelines. For measuring viscosity, LSM various concentrations (at pH 7.4) with 0.3, 0.5, and 0.7 % w/v were utilized. Mucilage was dissolved in purified water and put in a sonicator for three minutes. After that, the viscosity was determined at 37 °C using a Brookfield digital viscometer (model DE-V) (Ghumman et al., 2020).

2.4. Preparation of MTX-LSMCSNPs by polyelectrolyte complex method

Different quantities of polymers (LSM and CS) were used to make methotrexate nanoparticles, as shown in Table 1. Prepa-

ration of solution A (20 mL LSM was dissolved in distilled water) and solution B (20 mL CS was dissolved in 5 % glacial acetic acid) were done. Then solution A was added dropwise into solution B to prepare solution C, also called PEC (Polyelectrolyte complexes) solution by continuous stirring at 40 °C for 20 min, then at 50 °C for 5 min. For the preparation of MTX solution, dimethyl sulfoxide (DMSO) was used. 10 mg of MTX was solubilize in 10 mL of DMSO through continuous stirring performed by magnetic stirrer (Noreen et al., 2022). After that, the 5 mL of drug Methotrexate (MTX) solution was added drop wise using a syringe into the above-prepared solution C at 65 °C, with continuous stirring for 45 min. The samples were cooled and kept in sealed container. Prepared nanoparticles samples have been utilized for additional studies and characterization (Yousefpour P 2011).

2.5. Characterization of MTX-LSMCSNPs

2.5.1. Compatibility study by fourier transform infrared (FTIR) spectroscopy

FTIR spectra was acquired between 4000 and 500 cm^{-1} wavenumbers using the instrument IR Prestige-21 spectropho-

Table 1 Concentration of LSM (% w/v) and CS. (% w/v) for the Preparation of Nanoparticles.

S. No.	Formulation	LSM (%w/v)	CS(%w/v)	Drug(%w/v)
1	F1	0.01	0.01	0.05
2	F2	0.01	0.02	0.05
3	F3	0.02	0.01	0.05

tometer (Shimadzu, Kyoto, Japan) (Sindhu et al., 2015). For identification of the interaction between the drug and the polymers, spectral analysis of natural polymer used (LSM), synthetic polymer used (CS), pure drug (MTX), blank LSMCSNPs and MTX-LSMCSNPs were carried out by making a KBr disc.

2.5.2. Differential scanning calorimetry (DSC)

A thermal analyzer (Q600 SDT - TA, USA) was used to check the samples for thermal stability. Powdered samples were precisely weighed and placed on aluminum plates, temperature range of 50–400 °C was applied at 10 °C/min under a dynamic N₂ atmosphere. For the DSC thermograms, an empty pan was utilized as a reference (Ali et al., 2011).

2.6. Assessment of MTX-LSMCSNPs

2.6.1. Encapsulation efficiency of MTX-LSMCSNPs

MTX-LSMCSNPs were centrifuged at 4 °C for 45 min at 12000 rpm to separate the non-encapsulated drug to assess the encapsulation efficiency (EE). Measurement of absorbance at the wavelength of 306 nm was done using UV-spectrophotometer (Schimadzu, Japan UV-1650). To determine the amount of untrapped drug following equation was used (Ong et al., 2016, Bashir et al., 2021).

Encapsulation Efficiency

$$= \frac{(\text{Amount of total drug added}) - (\text{Amount of free drug})}{(\text{Amount of total drug added})} \times 100$$

2.6.2. Drug content and yield

MTX-LSMCSNPs (5 mg) were suspended in 0.5 mL of water, followed by the addition of 9.5 mL DMSO. Suspensions were centrifuged at 12000 rpm for 45 min at 4 °C under the chilling conditions to determine % yield and drug content. The nanoparticles pellet was dried after removing the supernatant. The % drug content and yield of MTX were calculated by UV-Spectrophotometer using the following equations (Gooneh-Farahani et al., 2020, Bashir et al., 2021).

$$\% \text{ Drug Content} = \frac{\text{Weight of drug in nanoparticles}}{\text{Weight of nanoparticles recovered}} \times 100$$

$$\% \text{ Yield} = \frac{\text{Weight of nanoparticles recovered}}{\text{Weight of total solid (polymers + drug)}} \times 100$$

2.6.3. Physical appearance

All the formulations prepared (F1, F2, and F3), of MTX-LSMCSNPs were checked visually for turbidity.

2.6.4. Zeta size and Zeta potential analysis

The particle size, polydispersity index (PDI), and zeta potential of the formulations F1, F2, and F3, of MTX-LSMCSNPs were evaluated using Malvern Instruments Nano ZS 90 Zeta-sizer (Malvern, UK). To eliminate repetitive scattering, a He-Ne laser and water as a dispersion were used (Refractive index: 1.33). Zeta potential and polydispersity index were also determined. Concentrated solution may lead to false results of particle size analysis due to multiple scattering. Therefore, 1 mg/mL of MTX-LSMCSNPs diluted solution was used for analysis. Data was analyzed by cumulant method of analysis in Malvern software. This software considered each particle as a sphere and considered that in bulk distribution. To avoid particle aggregation tendency, samples were added by using a 0.2 µm syringe filter. Collected results were averaged of thrice analysis of each formulation. Data obtained was also used for polydispersity index (PDI) analysis (Bhattacharjee 2016). PDI was calculated by dividing the square of standard deviation by the average particle diameter as mentioned in following equation.

$$PDI = \left(\frac{\sigma}{2d}\right)^2$$

2.6.5. Scanning electron microscopy (SEM) analysis

For surface and morphological analysis of MTX-LSMCSNPs, scanning electron microscopy (SEM) analysis was performed. Using a scanning electron microscope (SEM) (JEOL, IT100LA) with a 20- kV accelerating voltage, the form and surface morphology of contained Methotrexate loaded PEC stabilized NPs were studied. The small drop of NP suspension was dried on room temperature for 24 h as placed on SEM stub using double-sided adhesive tape and digital images of the samples were taken (Sahu and Das 2014).

2.6.6. Transmission electron microscopy (TEM) analysis

MTX-LSMCSNPs were also analyzed by Transmission electron microscopy. TEM analysis provides much higher resolution of nanoparticles image than other light-based techniques to analyze the quality, shape and size of nanoparticles. The picture was captured using a Transmission Electron Microscope (TEM) by placing the single drop of NP suspension to dry on room temperature on carbon-coated copper grids (CF400-Cu) (Hashad et al., 2016). The sample was examined using a TEM (Philips Technai-20) apparatus with a beam current of 104.1A and a voltage of 100 kV.

2.6.7. Swelling ratio of MTX-LSMCSNPs

To measure the swelling ratio weighed dried (Wd) samples of MTX-LSMCSNPs were immersed in phosphate buffer (37 °C) at different pH values for 24 h to attain equilibrium state. Samples were removed after 24 h, dried using filter paper

and weighed (Wg) again. Swelling ratio was calculated by using following formula.

$$\text{Swelling ratio} = \frac{W_g - W_d}{W_d}$$

2.6.8. *In vitro* drug release

The drug release from prepared MTX-LSMCSNPs formulations was checked by applying the dialysis bag approach using a dialysis membrane i.e., regenerated cellulose membrane (cut off 10,000kD). Dissolution rate apparatus, USP type-II (Pharma-Test, Hainburg, Germany) was used for this analysis. Formulations (containing 2.5 mg of MTX) were placed in a dialysis bag and then this bag was put in 250 mL dissolution medium (0.1 N HCL) and the study was carried out for 2 h. After this, the dissolution medium was replaced by 250 mL of another dissolving media (Phosphate Buffer pH 5.5 and pH 7.4), where they were studied for another 24 h at 37 °C with continuous stirring at a speed of 100 rpm. Studies were carried out at pH 5.5 to confirm the release rate in tumor microenvironment (Chickpetty and Raga 2013, Weng et al., 2020). At regular intervals of every 30 min, the 5 mL of sample was extracted and replaced with an equivalent volume of fresh dissolving media, then examined by UV-spectrophotometry at the wavelength of 306 nm. The concentration was obtained by the calibration curve of MTX at a given time (t) and release was determined by using the following equation (Kou et al., 2020).

$$\% \text{ drug release} = \frac{\text{Amount of MTX released}}{\text{Amount of loaded MTX}} \times 100$$

2.6.9. Kinetics of drug release

Different model-dependent approaches were employed to analyze the drug release kinetics from the controlled release formulation, including zero order, first order, Hixson–Crowell, Higuchi, and Korsmeyer–Peppas. The dissolution profiling of MTX-LSMCSNPs was carried out by applying these models via DDSolver software to ensure that the drug dissolution from the prepared formulations was occurring in an appropriate manner (Mircioiu et al., 2019).

Zero Order Kinetics: This model highlights that MTX-LSMCSNPs were at a concentration-independent release rate. The zero order kinetics is represented in following equation.

$$Q_t = Q_0 + K_0 t$$

Where Q_t signifies the amount of drug dissolved in time t, Q_0 the initial drug concentration in the solution, and K_0 the zero-order release constant (Libo and Reza 1996, Freitas and Marchetti 2005).

First-order kinetics: The model was used to explore the hydrophilic drugs release from a porous matrix and compared the drug content inside the drug carrier as represented as below.

$$\text{Log}Q_t = \text{Log}Q_0 - \frac{K_1}{2.303} t$$

Where, Q_t = amount of drug dissolved at time t; Q_0 = initial drug concentration in the solution. The first-order rate constant is denoted by K (Bravo et al., 2002, Ramteke et al., 2014).

Higuchi model: This model is mainly used to find out the cumulative percent release of hydrophilic drugs from poly-

meric matrixes of hydrophobic nature in relation to the square root of time as represented in the following equation.

$$Q_t = K_H \cdot t^{1/2}$$

Where, Q_t = amount of drug dissolved at time 't'; K_H = Higuchi model constant (Higuchi 1963, Grassi and Grassi 2005).

Hixson–Crowell model: The model explained the drug release changes by changes in surface area and diameter of the particles. Here drug release is linked to dissolution changes, not by diffusion and was determined using the following equation.

$$W_0^{1/3} - W_t^{1/3} = Kt$$

W_0 represents the initial drug quantity in the pharmaceutical dosage form, and W_t represents the drug quantity remaining in the pharmaceutical dosage form at time t (Chen et al., 2007).

Korsmeyer–Peppas Model: This model was used to explain the cumulative drug release from the polymeric matrix. The release rate constant for the Korsmeyer–Peppas model was calculated using the following equation.

$$\frac{Mt}{M_\infty} = Kt^n$$

Where Mt/M_∞ represents a drug-fraction released at time t, k represents the release rate constant, n represents the release exponent, and (kappa) represents a constant that integrates the surface volume relationship.

2.7. Stability studies

The development of crystals for prepared formulations was monitored from the 1st, 7th, 14th, and up to the 30th days. The size and encapsulation efficiency of the MTX-loaded LSMCSNPs were measured at room temperature up to one month to ensure the stability of prepared nanoparticles (Malviya et al., 2021).

2.8. Acute toxicology study

The MTD (Maximal Tolerance Dose) approach was used to analyze MTX-LSMCSNPs for acute oral toxicity research. Swiss albino mice (28–32 g) of both sexes were bought from the animal laboratory at the University of Sargodha (UOS). All experiments were carried out following OECD rules, and the ethics committee of UOS (Ref. No. 20B22IAEC–2022/PREC) double-checked them. Two groups (control and treatment) with an equal number of male and female mice (n = 8) were maintained in a clean housing facility with a 12-hour light/dark cycle and regular food plus water. Only the treatment group received LSMCSNPs of MTX (10 mg/kg) through tail vein. The dose of LSMCSNPs of MTX was according to the criteria as used for excipient toxicity testing. All details linked to the indication of toxic effects, bad health, mortality, and any other activity effect were noticed in all animals for two weeks, twice daily.

Hematological and clinical biochemistry analyses were performed after the completion of two weeks. Overall, the treated group was compared with the controlled group for each parameter. Using an Olympus AU2700 Chemistry analyzer®,

plasma was separated and examined for several clinicopathological studies (Olympus Optical, Tokyo, Japan). Hepatic (ALT, AST) and renal (creatinine, urea) analyses were also performed and compared to primary reference procedures according to the IFCC (International Federation of Clinical Chemistry and Laboratory Medicine) (Bhattacharya 2020).

2.9. Cell viability assay

The cell viability assay was carried out for the assessment of biomedical applications of the prepared formulation. The *in-vitro* cytotoxicity of LSMCSNPs was evaluated by MTT assay by using HepG2 and MCF-7 cell lines. The cell line was grown in Dulbecco's Modi-field Eagle Medium (DMEM), in 10 % of FBS (Fetal Bovine Serum) and has four times more concentration of amino acids and vitamins than the standard medium. The cells were dispersed at 37 °C in a 5 % CO₂ atmosphere before being sowed into 96 well plates (1x10⁴ cells per well) and incubated for 48 h. Dimethyl sulfoxide (DMSO) at a concentration of 500 µg/ml was used to dissolve the test samples, which was further diluted by using water to 200 µg/ml and then kept in the frozen state for later use. Frozen samples were defrosted and diluted with LSMCSNPs (3.12, 6.25, 12.5, 25, 50, and 100 µg/ml) before being incubated with culture plates for 48 h. The cell lines were likewise treated with the same concentrations of pure MTX. 100 µL of MTT along with 5 mg/ml concentration of formulation was put in each well and incubated for 4 h. To dissolve the crystals, culture media was replaced with DMSO in each well. The absorbance was measured using a microplate reader (Thermo Fisher Scientific, Rockford, IL, USA) at wavelengths 570 nm and 650 nm (Aluigi et al., 2018a, 2018b). The experiment was carried out three times and results are represented in mean ± S.D. Cell viability results were calculated by using the mentioned equation below.

$$\text{Cell viability} = \frac{\text{Testcells}_{abs}}{\text{Controlcells}_{abs}} \times 100$$

2.10. Cell apoptosis assay

Cell apoptosis analysis was carried out via flow cytometry technique. For 24 h, MCF-7 cells were incubated with MTX-LSMCSNPs. After a 12-hour incubation period at 4 °C, the cells were rinsed with PBS and fixed with ethanol (70 %). After

this, centrifugation was done and the pellets were treated with propidium iodide (PI) 50 µg/ml i.e., a fluorescence probe solution and then with FITC-labeled annex-V (1 mg/ mL). After that, the plate was placed in the dark for 15 min. Fluorescence was detected at 495–535 nm (excitation) and 519–617 nm (emission) wavelengths for PI and FITC labeled annex-V, respectively, using a FACS caliber flow cytometer (Becton, Dickinson, Franklin Lakes, NJ, USA) (Afshari et al., 2014, Chaudhari et al., 2021a, 2021b).

2.11. Statistical analysis

Every test and procedure was repeated in triplicate manner and presented as mean ± S.D. The obtained data were statistically analyzed by one-way ANOVA, p less than 0.05 alongside a Tukey posthoc test to evaluate the significant variations, if presented between independent variables. Graph-Pad Prism 8.2 was used for the analysis of data and making graphs. DDSolver software was used to generate R₂ and MSC values to validate the accuracy and prediction capabilities of several kinetic models.

3. Results and discussion

The key aspects of cancer therapies are low absorption and compatibility with normal cells. The use of effective technologies for encapsulating cancer medications with biopolymers appears to offer alternatives to these deficiencies. Due to their nontoxic, biodegradable, and versatile characteristics, LSM and CS have been selected as potential carriers for MTX administration. Complexes were formed because of cross-bridging between LSM (anionic polymer) and CS (cationic polymer), as seen in Fig. 2. Because of the strong connection between the two polyelectrolytes, numerous electrostatic interactions throughout the CH strands were produced, resulting in a significant polyelectrolytic complex formation. Moreover, nano sized systems were created using high-intensity ultrasonography by creating sonic holes in the water phase. The goal of this work was to develop LSM-CS-based compositions that might allow chemotherapeutics to be included in the maximum pharmacological activity in a controlled manner while reducing their toxic effects. Furthermore, encapsulating MTX using LSM might make it possible to distribute the nanoparticles orally because it would protect them from the gastrointestinal region. Numerous compositions (F1, F2, F3)

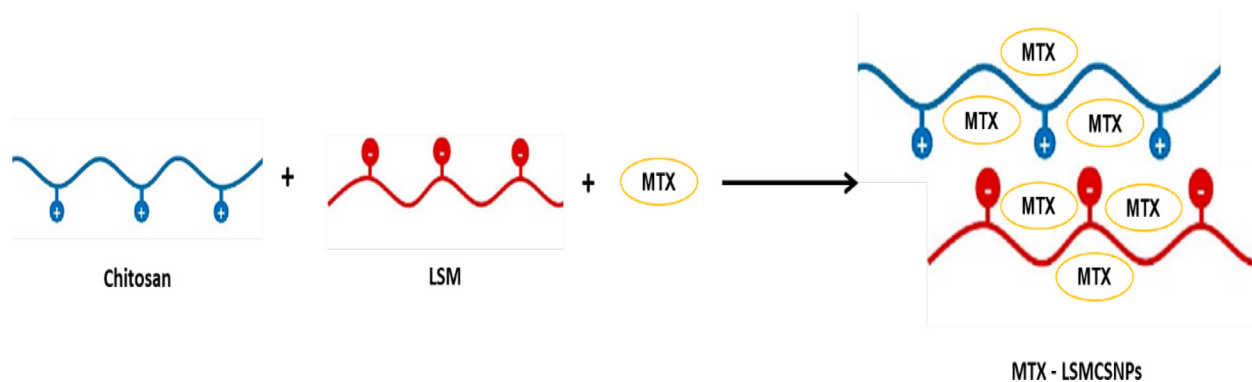


Fig. 2 Schematic representation of PEC formation between MTX loaded LSM and CS NPs.

S. No.	Parameters	LSM
1	Percentage yield (%)	7.4 %
2	pH of mucilage	7.2 ± 0.33
3	Solubility	Soluble in hot water Swollen in cold water
4	Apparent Viscosity at same shear rate	47.8 cp ± 2.6
	Conc. of LSM 0.3 %	105.7 cp ± 3.1
	Conc. of LSM 0.5 %	574.2 cp ± 1.3
	Conc. of LSM 0.7 %	

containing different proportion of LSM and CS in ratios of 1:1, 1:2, and 2:1 were developed for it.

3.1. Physicochemical properties of LSM

Using ripe and matured Linseeds, mucilage (LSM) was isolated, and a 7.4 % yield of pure LSM was obtained and used for the preparation of all three samples. LSM was swollen in cold water; though was solvable in hot water. The pH of extracted mucilage was 7.2. The apparent viscosity of mucilage has been assessed using the range of concentrations of 0.3 to 0.7. At the same shear rate, the apparent viscosity was 47.2, 105.7 and 574 cp at the concentrations of 0.3, 0.5 and 0.7 respectively as shown in Table 2 (Ghumman et al., 2020).

3.2. Characterization of MTX-LSMCSNPs

3.2.1. Fourier transform infrared (FTIR) spectroscopy

The FTIR spectra of MTX, CS, LSM, blank LSMCSNPs and MTX-LSMCSNPs was shown in Fig. 3. The IR spectra of the MTX (Fig. 3a) showed absorption bands at 3338 cm⁻¹ (O—H stretching), 3080 cm⁻¹ (N—H stretching), 1670–1600 cm⁻¹ (C=O stretching), 1550–1500 cm⁻¹ (N—H bending), 1400–1200 cm⁻¹ (C—O stretching), 930 cm⁻¹ (O—H bending), and 820 cm⁻¹ (C—H bonding) (Boni et al., 2018, Nosrati et al., 2018, Gao et al., 2021). The spectra of CS (Fig. 3b) showed the peak of the OH group at 3356–3284 cm⁻¹, the peak of —CH₂ stretch at 2921 cm⁻¹, the peak of C=O stretching at 1651 cm⁻¹, the peak of —CH₂ bend at 1430–1384 cm⁻¹, the peak of N—H at 1592 cm⁻¹, the peak of C—O—C glycoside linkage at 1154 cm⁻¹, and the peak of Carbonyl, C—O at 1070 cm⁻¹ (Ahyat et al., 2017, Priya et al., 2020). The IR spectrum of LSM (Fig. 3c) revealed a larger band for —OH group stretching, ranging from 3674.39 cm⁻¹ to 3332.92 cm⁻¹; —CH₃ was being stretched at 2856.23 cm⁻¹ (Kurra et al., 2019). It moreover exhibited significant bands for —CH group stretch at 1685.06 cm⁻¹ (Ghumman et al., 2020). Other notable features include a sharp peak at 1440.83 cm⁻¹ owing to —CH stretching, a characteristic peak at 1112.95 cm⁻¹ due to glycosidic bond (C—O—C) of polysaccharide, and a characteristic peak at 1037.20 cm⁻¹ due to —CO bending (Rocha et al., 2021). The spectra of blank LSMCSNPs (Fig. 3d) showed the peak of the OH group at 3274 cm⁻¹, the peak of —CH₂ stretch at 2126 cm⁻¹, the peak of C=O stretching at 1634 cm⁻¹, the peak

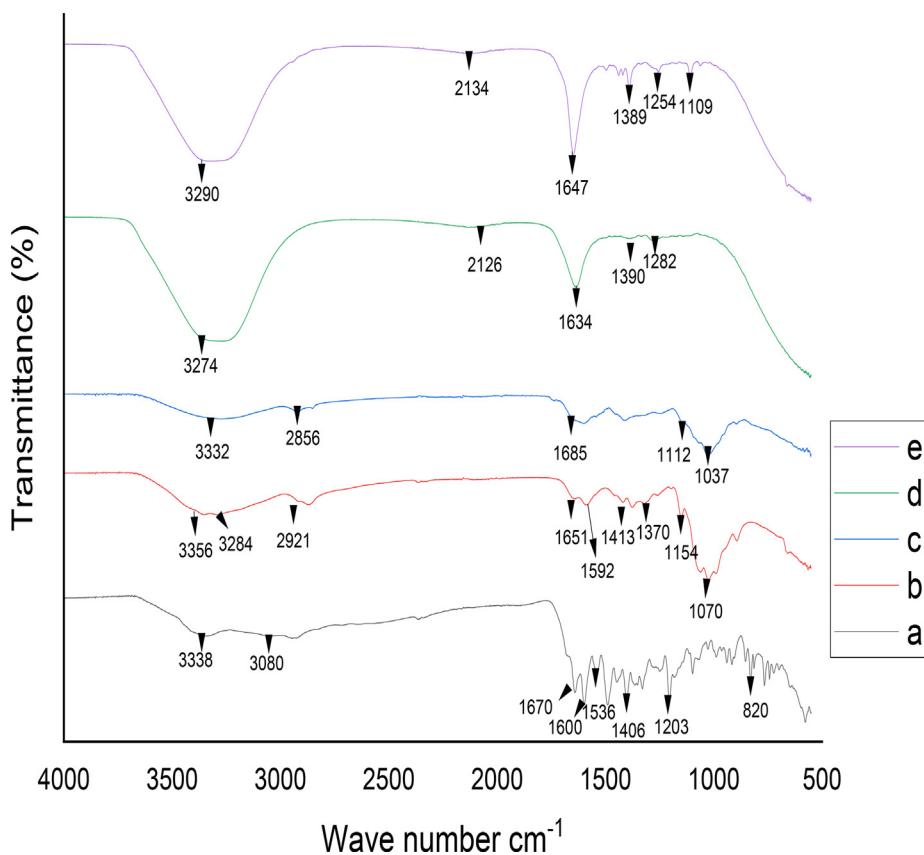


Fig. 3 Drug polymer compatibility FTIR studies (a) MTX (b) CS (c) LSM (d) Blank LSMCSNPs (e) MTX-LSMCSNPs.

of $-\text{CH}_2$ bend at 1390 cm^{-1} , $\text{C}-\text{O}-\text{C}$ glycoside linkage represents a peak at 1282 cm^{-1} , and the peak of Carbonyl, $\text{C}=\text{O}$ at 1070 cm^{-1} . The IR spectra of MTX-LSMCSNPs (Fig. 3e), showed absorption bands at 3290 cm^{-1} that was linked to $\text{O}-\text{H}$ stretching, the peak of $-\text{CH}_2$ stretch at 2126 cm^{-1} , $1640-1600\text{ cm}^{-1}$ represented $\text{C}=\text{O}$ stretching, $1550-1500\text{ cm}^{-1}$ showed $\text{N}-\text{H}$ bending, $1400-1100\text{ cm}^{-1}$ was linked to $\text{C}-\text{O}$ stretching. Furthermore, IR spectra exhibited a shifting in the $\text{COO}-$ peak shift to 1647 cm^{-1} , suggesting the formation of electrostatic bonds between two LSM and CS. The results revealed that the functions of the physical mixture of MTX, LSM, and CS do not interact.

3.2.2. Differential scanning calorimetry (DSC)

LSM bears three endothermic and one shoulder peak (Fig. 4a); a high denaturation temperature of $114.7\text{ }^\circ\text{C}$ was observed. Melting point and oxidation temperature were shown at $55-56\text{ }^\circ\text{C}$ and $146-153\text{ }^\circ\text{C}$ respectively (Athukorala et al., 2009). The DSC thermogram of CS (Fig. 4b); revealed a large exothermic peak at $297\text{ }^\circ\text{C}$; the degradation of chitosan amine units was linked to this exothermic peak. Chitosan has shown an endothermic peak at $80\text{ }^\circ\text{C}$. This endothermic peak was related to the hydrophilic groups of chitosan associated with the loss of water (Dey et al., 2016). The DSC thermogram of MTX showed two endothermic peaks $129\text{ }^\circ\text{C}$ due to release of water and (Fig. 4c); and broad endothermic peak in the range of $195-210\text{ }^\circ\text{C}$ has showed the melting point of pure MTX (Taberi et al., 2011, Ray et al., 2015, Toomari and Namazi 2016). In MTX-loaded nanoparticles thermogram

(Fig. 4e), it was observed that the melting point of MTX was shifted towards a lower temperature. It could be because MTX was not in crystalline form, but was in an amorphous state (Fini et al., 2010).

3.3. Evaluation of MTX-LSMCSNPs

3.3.1. Encapsulation efficiency, drug content and yield

Methotrexate-loaded PEC stabilized nanoparticles based on LSM-CS were found to have drug entrapment efficiency (%) ranging from 49.97 ± 0.91 to $72.25 \pm 0.66\%$. The % drug content was determined to be between 82.52 ± 0.95 and $92.83 \pm 0.72\%$, while the % yield was found to be between $72.33 \pm 1.01\%$ and $88.08 \pm 0.88\%$ as shown in Table 3. With increasing LSM concentrations, the entrapment efficiency, drug content, and yield all improved. Because the quantity of LSM in formulations F1 and F2 (1:1) and (1:2) was equal, there was little variation in the outcomes. LSM-CS content was increased in formulation F3 (2:1) which might be due to adequate interaction between the viscous LSM solution and chitosan does not allow the drug to leach out of loosely aggregated polyelectrolyte particles.

3.3.2. Physical appearance

All MTX-LSMCSNPs formulations were colorless and transparent. No apparent particulates or turbidity was seen. The formed nano-suspensions were found to be clear with no signs of precipitation.

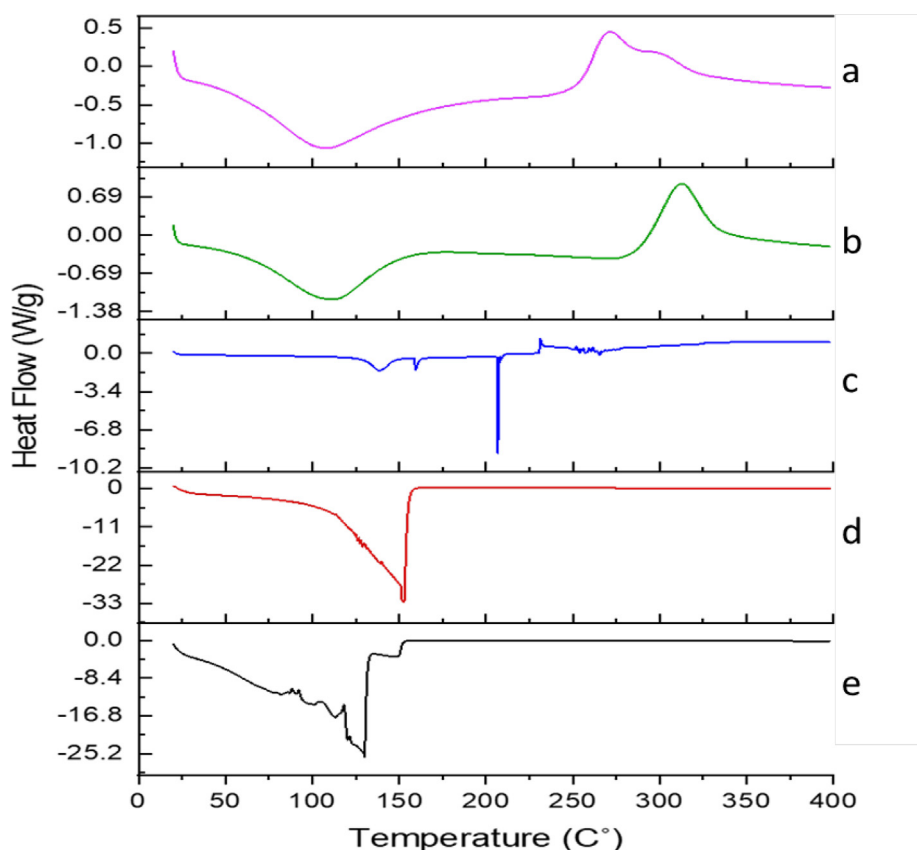


Fig. 4 Differential scanning calorimetry (DSC) Thermogram (a) LSM (b) CS (c) MTX (d) Blank LSMCSNPs (e) MTX-LSMCSNPs.

Table 3 Encapsulation efficiency (% EE), Drug content and percent yield of MTX-LSMCSNPs in mean \pm standard deviation (S.D.)/ n = 3.

Formulation	LSM:CS (Mass Ratio)	% Entrapment Efficiency	% Drug content	% yield
F1	1:1	49.97 \pm 0.94	86.02 \pm 1.19	76.19 \pm 0.87
F2	1:2	54.98 \pm 1.08	82.52 \pm 0.95	72.33 \pm 1.01
F3	2:1	72.25 \pm 0.72	92.83 \pm 0.72	88.08 \pm 0.88

3.3.3. Particle size distribution and morphology of nanoparticles

The size distribution and ζ -potential values of MTX-LSMCSNPs are shown in Table 4. The particle size was determined to be between 192.1 nm and 246.6 nm, with a PDI of 0.326 to 0.502. The smallest particle size (192.1 nm) was found in formulation F3, which might be associated with the lowest CS content and highest LSM concentration. Formulation F3 with zeta potential -16.6 mv, which might be related to the lowest CS content and greatest LSM concentration, as the chitosan is cationic and LSM is anionic in nature. Formulation F2 with zeta potential of $+ 9.8$ mv, which might be due to the high CS content that, is cationic in nature. The polydispersity index (PDI) tells us the heterogeneity in the detected particle size. PDI is a dimensionless parameter and if the value of PDI is less than 0.1, then particles are considered as “Monodisperse” and particle size is considered “Polydisperse” with PDI value, greater than 0.7 (Souza et al., 2016, Danaei et al., 2018). As evidenced by our samples; PDI was from 0.3 to 0.5; all samples showed suitable particle size distributions (values below 0.5), they also show a comparatively less susceptibility of agglomeration (Dantas et al., 2018). Dynamic light scattering (DLS) analysis was done to calculate the PDI results. Particle size was smallest when the LSM-CS ratio was 2:1. Changes in the mass ratio of LSM and CS resulted in a shift of particle size and showed that the LSM-CS ratio affects the particle size (Bhattacharya 2020). Secondly, ζ -potential was reduced upon increasing the ratio of LSM to Chitosan (Fig. 5A & B). SEM analysis and chemical composition of LSM was also checked (Fig. 5C & 5G). Further, SEM and TEM analysis for the formulations (F1-F3) along with their respective histogram are shown in (Fig. 5D-5F), representing the size distribution of nanoparticles. In Fig. 5F, particle size was measured by SEM image using ImageJ software for F1, F2, F3 formulations. SEM and TEM analysis showed that all MTX-LSMCSNPs had solid, smooth, and nearly spherical shapes (Noreen et al., 2022). The mean size distribution of NPs was in accordance to DLS analysis which was confirmed by applying the Gaussian fit of counts on distribution frequency (Souza et al., 2016). DLS analysis revealed the particle size distribution but SEM and TEM analysis was

done to see the exact shape of MTX-LSMCSNPs and more reduced size had been seen at a ratio of 2:1 (Fig. 5D-F).

3.3.4. pH-dependent swelling behavior of MTX-LSMCSNPs

pH of the medium is the most important factor that affect the swelling of behavior of nanoparticles, so swelling behavior was checked at various pH values and results have been plotted in Fig. 6. At acidic pH the amine groups with in polymeric layer of the LSM-CS having positively charged and thus protonated so an increase in swelling ratio results from the ensuing repelling force. Swelling ratio diminished when the pH was raised to a neutral level. It was anticipated to be have minimal surface charges because of this reduced swelling ratio values. Nevertheless, the trend towards higher pH levels (i.e., basic condition), swelling ratio grew once again, that specified most likely as a result of the medium’s increased ion concentration (Najafipour et al., 2020).

3.3.5. Drug release studies

For the proper treatment of cancer disease, tumor- targeted drug delivery is required with minimum or no release of drug before the targeted site. Otherwise, the first pass effect can reduce the efficacy of the drug and leads to failure of treatment. Therefore, sustained and targeted delivery of hydrophobic drugs is required with maximum efficacy and minimum toxicity. The diffusion bag technique was used to achieve *in-vitro* drug release, and data were collected for all the prepared MTX-LSMCSNPs formulations. The release studies were carried out both at normal simulated conditions (pH 1.2 and pH 7.4) and pH linked to the tumor microenvironment (pH 5.5). At pH 1.2, all formulations showed drug release within the range of 8 to 14 % and results were insignificant between all formulation (F1, F2 and F3). At pH 5.5, cumulative % release was 58–69 %, while at pH 7.4, it was recorded around 47–58 % up to 24 h. The drug released quickly at pH 5.5, due to protonation of carboxyl and amino groups present on LSM-CS surface enhanced the swelling capacity of both polymers. Faster release at pH 5.5 was also due to repulsion happened between similar charges. Whereas at pH 7.4 release

Table 4 Characterization of MTX-LSMCSNPs.

Formulation	LSM:CS (Mass Ratio)	Characterizations			
		Physical Appearance	Particle Size	PDI	Zeta Potential
F1	1:1	Clear Solution	244.9 nm	0.326	+ 1.2 mv
F2	1:2	Clear Solution	246.6 nm	0.502	+ 9.8 mv
F3	2:1	Clear Solution	192.1 nm	0.363	-16.6 mv

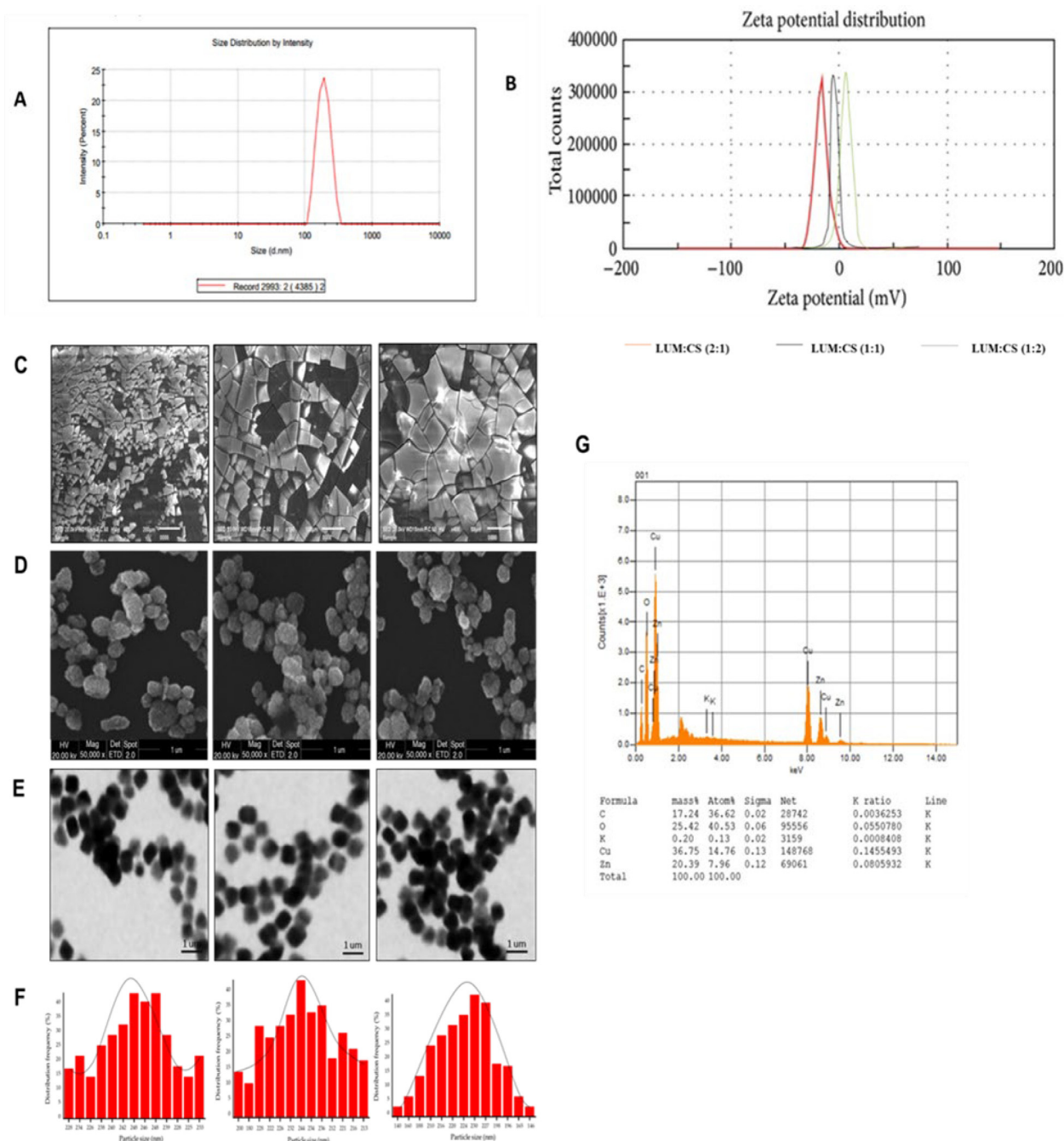


Fig. 5 (A) Zeta-average d.n.m of F3 (LSM-CS in ratio (2:1)) (B) Zeta-potential (mV) of F3, F2, F1 of LSM:CS ratio (2:1, 1:2 and 1:1). (C) Chemical composition of LSM (D) SEM images of LSM (E) SEM images of F3, F2, F1 LSM:CS ratio (2:1, 1:2 and 1:1) (F) TEM images of F3, F2, F1 of LSM:CS ratio (2:1, 1:2 and 1:1). (G) Size distribution histograms of F3, F2, F1 of LSM:CS ratio (2:1, 1:2 and 1:1).

was slow as the swelling index was low due to deficient surface charges (Najafipour et al., 2020). The *in vitro* release data indicated that the MTX-LSMCSNPs formulation showed sustained drug release with a steady rise as shown in Fig. 7. Overall, the F3 formulation had superior and sustained drug release than F1 and F2 due to a higher concentration of LSM than chitosan. On the other hand, in the F2 formulation, the percentage of drug release was reduced due to higher concentration of chitosan than LSM. Whereas, F1 formulations

exhibited a percentage drug release between the F2 and F3 formulations due to equal concentrations of LSM and chitosan.

While constructed like a nanoparticles systems, MTX-LSMCSNPs formulations (F3) with smaller particle size showed higher *in vitro* therapeutic characteristics in the dissolution experiment. The impact of therapeutic substance-loaded dosage forms with decreased particle size on dissolution rate has subsequently become the subject of extensive research (Takano et al., 2008). That enormous surface region enabled

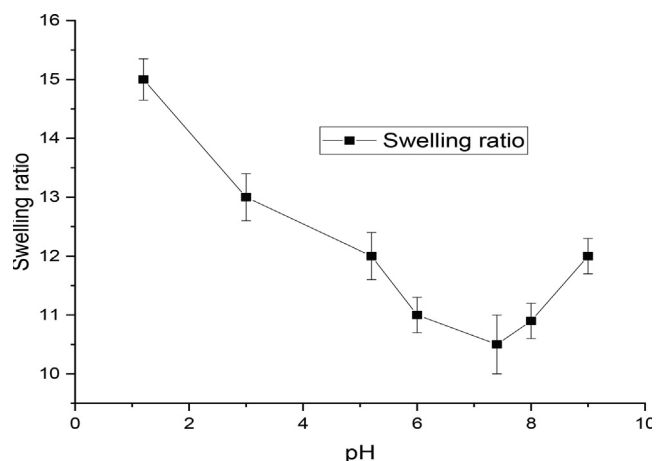


Fig. 6 Swelling ratio of MTX-LSMCSNPs at various pH values.

through fabricating the hydrophobic constituents using nanoparticle systems resulted for the *in vitro* disintegration behavior being consistent with certain other biological molecules, which facilitated drug solubility through achieving fast immersion throughout the container (Hintz and Johnson 1989). The hydrophobic substance was reduced to such nanometer size because of a rise in molecule curving, which also resulted in a rise in dissolving pressures. Greater permeability due to the reduced size permitted for increased drug absorption concentrations. That results in enhanced physical and chemical qualities and therefore should resolve the *in vivo* permeation issue with the poorly soluble MTX as BCS class II drugs (Mauludin et al., 2009, Kou et al., 2020).

3.3.6. *In-vitro* drug release kinetics

Five different model-dependent kinetic approaches were employed to analyze the drug release kinetics from the of MTX-LSMCSNPs. DDSolver software was used to study that the drug release kinetic behavior from the prepared formulations (Mircioiu et al., 2019). The findings are summarized in Table 5. All of the formulations of MTX-LSMCSNPs (F1, F2, and F3) followed the Higuchi model at both pH 5.5 and pH 7.4, with the highest R^2 values as compared to all other models. R^2 values were near to one that represents these MTX-LSMCSNPs formulations following the Higuchi model approach. Higuchi model approach is chiefly used for studying the drug release kinetic from the nanoparticles formulations. The Higuchi model is generally linked to three types of hypothesis. Firstly, drug concentration is higher initially than drug solubility. Secondly, the drug particles are encapsulated inside the nanoparticles having no drug on the surface of the nanoparticles, because the particles are much smaller than the thickness of the prepared system. Thirdly, this Higuchi model follows the porous system because hydrophilic polymer solubilizes easily to create pores, drug diffusivity remains constant and drug release occurs through pores created in the matrix (Mircioiu et al., 2019). Further, we checked the data by Korsmeyer-Peppas model that showed the second highest R^2 values as compared to other models after the Higuchi model and N value of F1 and F2 formulations was between 0.45 and 0.89, representing the non-fickian transport while F3 formulation, has N value less than 0.45, representing the fickian transport at pH 5.5 and N value for all formulations (F1, F2, and F3) was less than 0.45 at pH 7.4, representing fickian transport behavior for drug release.

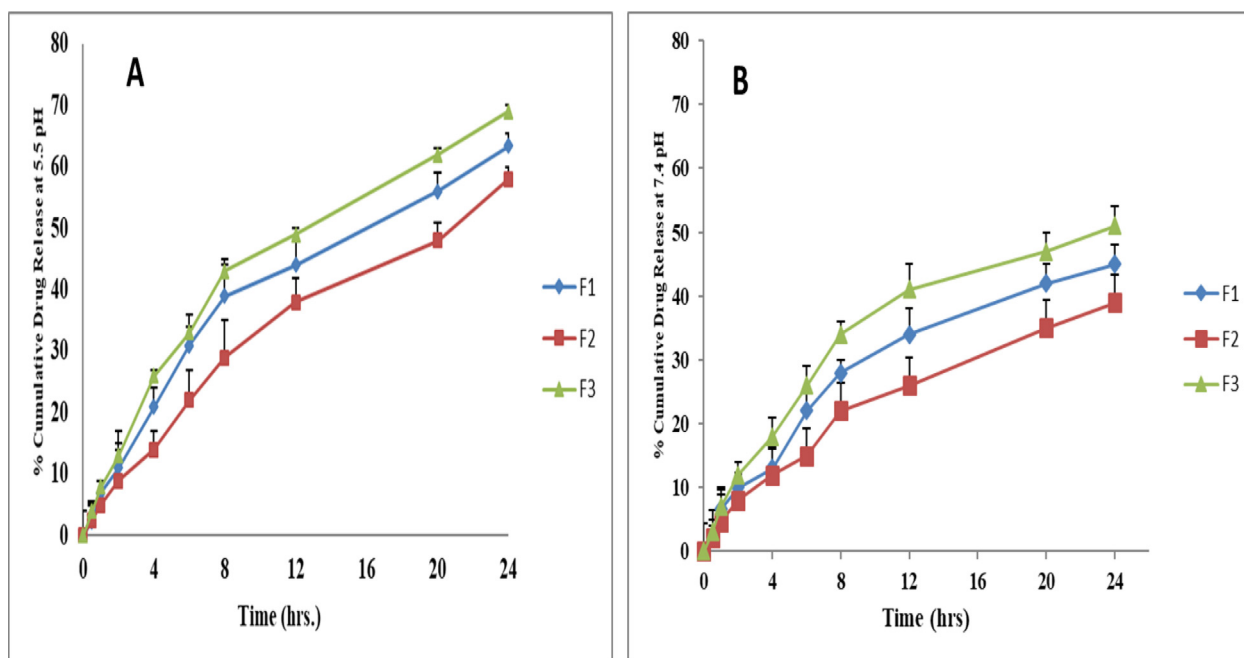
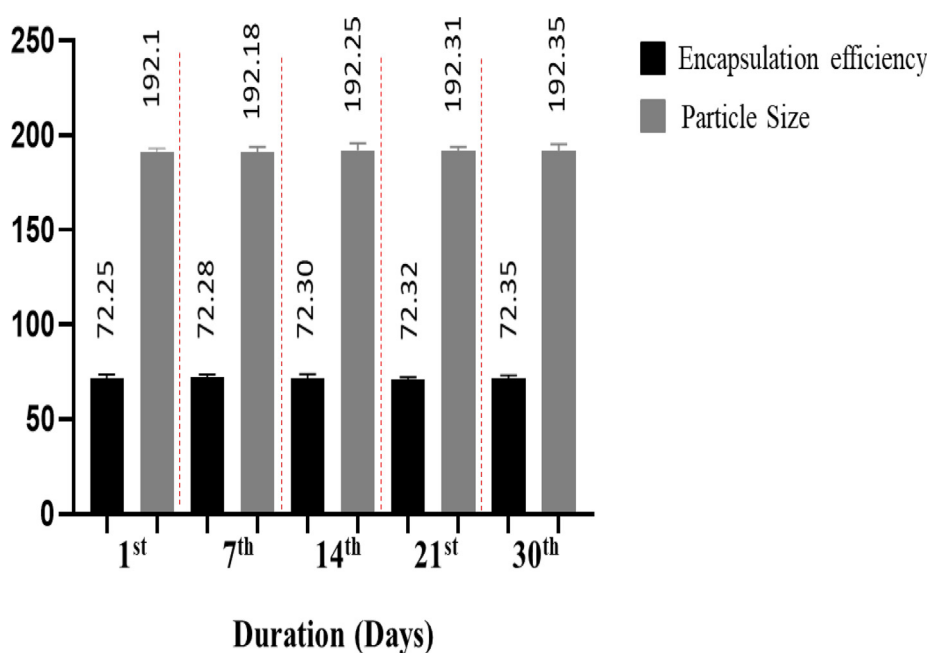


Fig. 7 *In vitro* cumulative drug release percentage, (CDR %) of MTX-LSMCSNPs (A) pH 5.5, (B) 7.4 at 37 °C. (n = 3/ Mean ± S.D.).

Table 5 (A) Modelling and release kinetics of nanoparticles at pH 5.5. (B) Modelling and release kinetics of nanoparticles at pH 7.4.

Nanoparticle	Zero order		First order		Hixson-crowell		Higuchi		Korsemeyer peppas		
	R ²	K ₀	R ²	K ₁	R ²	K _{HC}	R ²	K _H	R ²	K	n
F1	0.3367	1.4741	0.3938	0.019	0.4160	1.1083	0.8647	6.85	0.7499	11.02	0.461
F2	0.4461	1.5286	0.4986	0.029	0.5133	1.1332	0.8755	9.26	0.8203	12.44	0.458
F3	0.4997	1.2567	0.6139	0.023	0.5170	1.2459	0.9423	11.42	0.8937	6.544	0.528

Nanoparticle	Zero order		First order		Hixson-crowell		Higuchi		Korsemeyer peppas		
	R ²	K ₀	R ²	K ₁	R ²	K _{HC}	R ²	K _H	R ²	K	n
F1	0.4372	2.4007	0.6562	0.034	0.5269	1.4817	0.8284	6.79	0.8925	9.92	0.399
F2	0.4379	1.6147	0.7101	0.026	0.6619	1.6787	0.9544	9.39	0.9092	8.56	0.328
F3	0.6476	2.1296	0.7686	0.044	0.7932	1.8358	0.9713	11.52	0.9242	12.33	0.360

**Fig. 8** Stability studies of MTX-LSMCSNPs (F3 formulation; LSM: CS in a ratio of 2:1) over a time duration of 1 month in mean \pm S. D (n = 5).

3.4. Stability studies

The size and encapsulation efficiency of the MTX-LSMCSNPs were measured at room temperature for one month to ensure stability. Data were first gathered daily, then on a weekly basis (Fig. 8). During the study period, no growth and no significant variation in the size of nanoparticles was seen or the encapsulation effectiveness of the formulation (F3), indicating the stability of the encapsulation layer for MTX- LSMCSNPs.

3.5. Acute toxicological study

Over the course of two weeks following the completion of this acute research, no deaths were seen in either the control or the

treatment groups. During the monitoring period, no changes in appearance or signs of sickness were seen in any of the mice. In both groups, changes in body weight were minor (Fig. 9A). Both groups' essential organs, such as the heart, liver, spleen, kidney, and stomach, were undamaged. Both the treatment and control groups consumed the same amount of food and drink, indicating a normal physiological state. Acute toxicological experiments were conducted using Swiss albino mice to examine side effects and lethal (LD50) values of testing compounds in line with a worldwide-harmonized system to determine toxicity scores equal to zero. As a result, our MTX-LSMCSNPs formulation corresponded to the above-mentioned group, which had a zero toxicity score. The greatest technique to evaluate chemical toxicity created under physio-

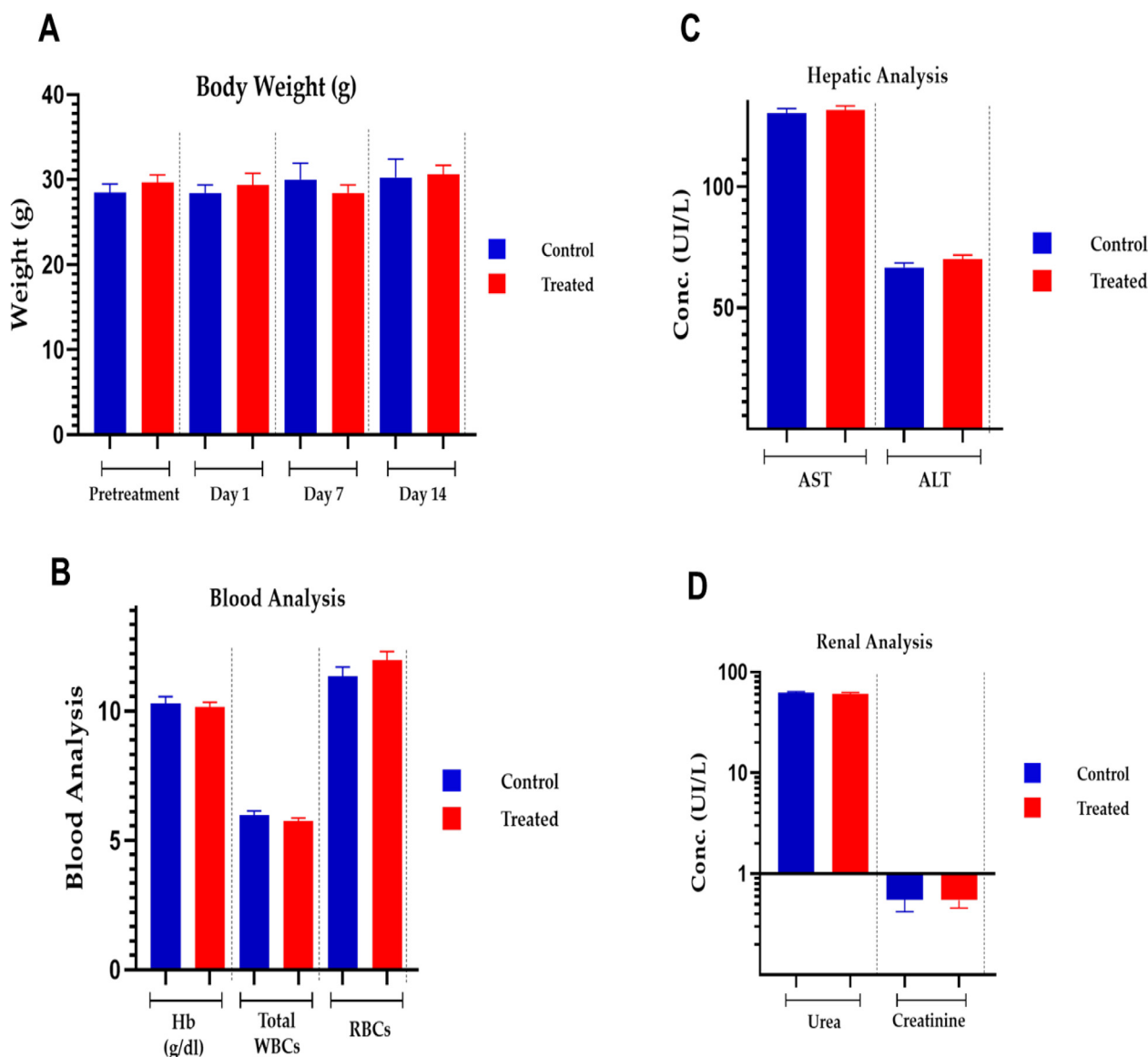


Fig. 9 Acute toxicological analysis of MTX-LSMCSNPs (F3 formulation).

logical and pathological settings is to use blood plasma. Fig. 9 B, C, and D showed plasma examination of several chemical parameters related to liver and kidney function in both the control and treatment groups. Both groups' ALT and AST values were determined to be within the reference range and similar. Aside from ALT and AST, creatinine and urea levels were found to be within acceptable limits. In both groups, these measurements showed no signs of toxicity in the blood, liver, or kidney (Shafiq et al., 2022).

3.6. Cell viability assay

Cell viability test was performed of MTX-LSMCSNPs (F3) on Vero (normal cells), HepG2 and MCF-7 cell lines for 48 h. Samples were observed at 0, 24, and 48 h (Fig. 10). MTX-LSMCSNPs considerably reduced cancer growth for both HepG2 and MCF-7 cell lines, whereas there was no significant

cytotoxic effects on cell viability in case of Vero cell lines. The drug is anticipated to grow progressively, therefore at 24th and 48th hour a remarkable high cellular cytotoxicity for both cell lines (blackened cells) was observed (Aluigi et al., 2018a, 2018b). Therefore, as assessed to numerous described earlier nanomaterials for MTX, the cytotoxic effects appeared notable. Therefore, more in-vivo research is necessary to completely comprehend MTX's anticancer activity.

3.7. Cell apoptosis assay

The cell apoptosis experiments were performed as indicated in the methodology to better understand the mechanism of improved antitumor activity by MTX-LSMCSNPs. Fig. 11A & B showed the apoptotic outcomes of MCF-7 cells pretreated with PBS, pure MTX, and MTX-LSMCSNPs up to 12 h. In MCF-7 cells, Simple free MTX generated a modest rate of

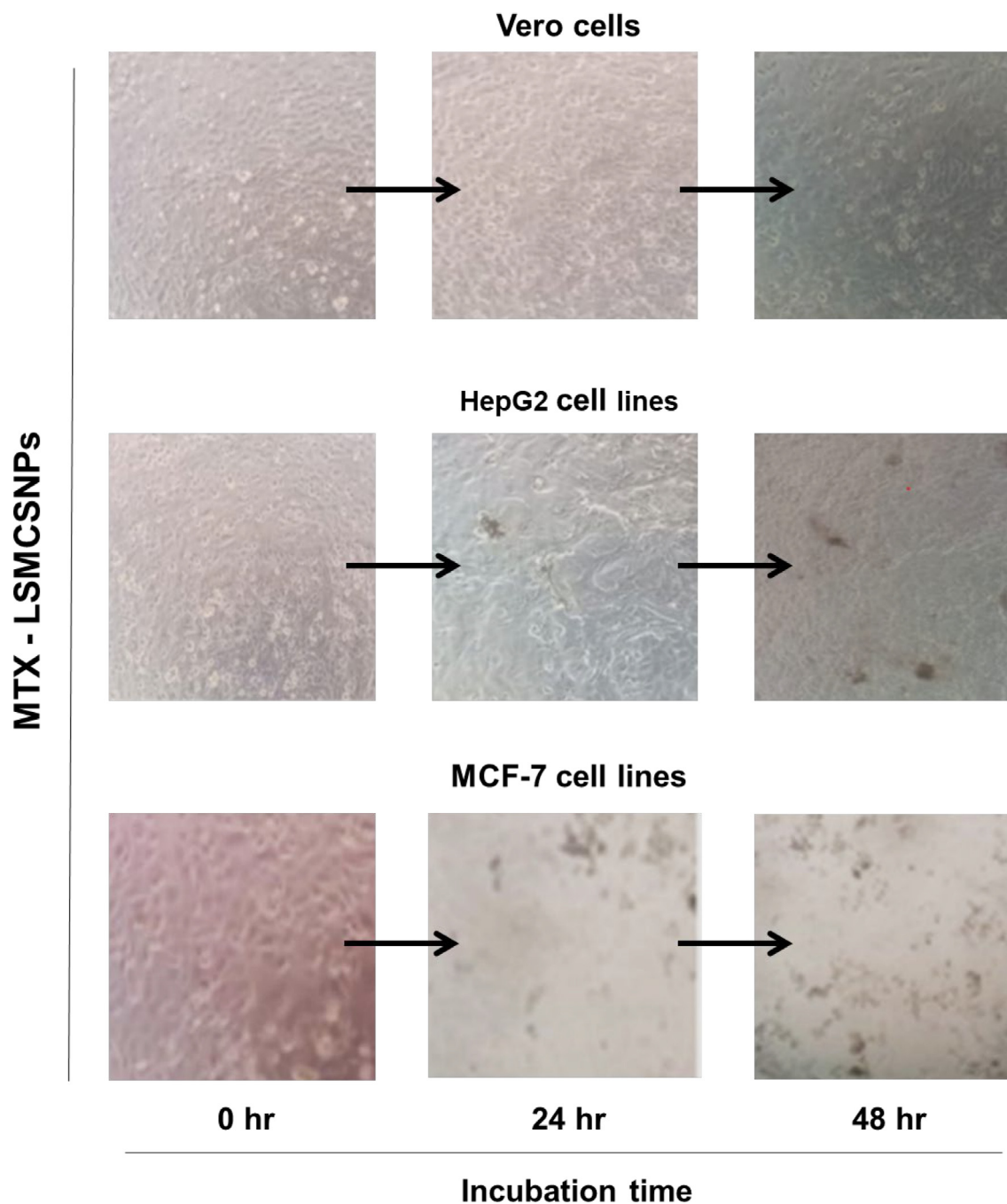


Fig. 10 Representative images of Vero (normal cells), HepG2 and MCF-7 cancerous cells upon treatment with F3 formulation (Scale bar = 1 mm).

apoptosis. However, MCF-7 cells treated with MTX-LSMCSNPs had a significantly greater rate of apoptosis (21.2 %) than those treated with MTX alone (14.14 %). These findings suggested that the targeting and sustained ability of MTX-LSMCSNPs is responsible for increased drug uptake

or penetration by cells over a longer length of time, resulting in a distinct difference in apoptosis levels. MTX- LSMCSNPs, on the other hand, may have a greater benefit in reducing the toxic side effects of nanodrugs through prolonged targeted administration (Chaudhari et al., 2021a, 2021b).

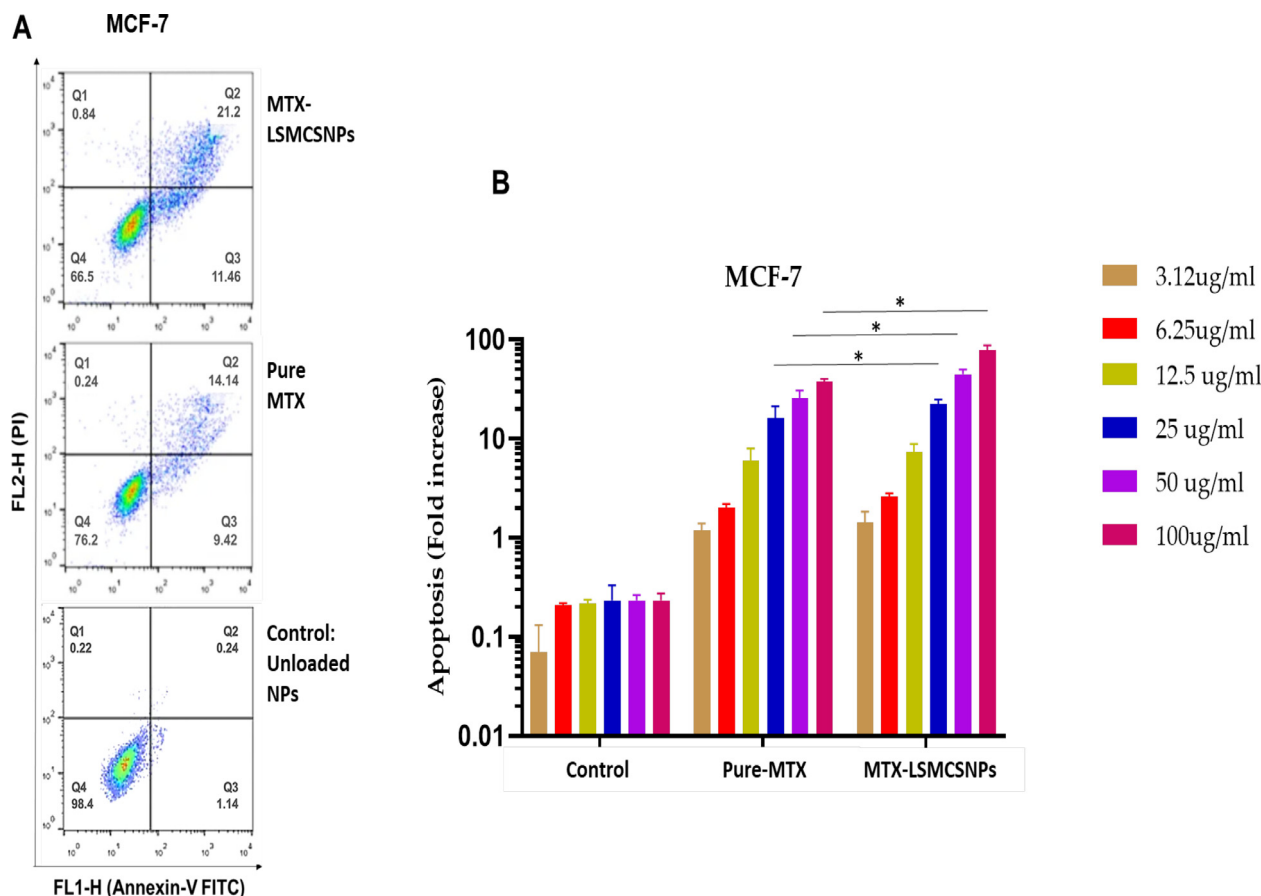


Fig. 11 Cell apoptosis analysis on MCF-7 cell lines **A**). Flow cytometry dot plot representing MCF-7 cells treated with unloaded LSMCSNPs, pure MTX and MTX-LSMCSNPs (F3 formulation) **B**) Quantitative apoptosis (Fold increase) analysis of MTX-LSMCSNPs (F3), with pure MTX, and unloaded LSMCSNPs on MCF-7 cancer cell lines (3.12, 6.25, 12.5, 25, 50, and 100 $\mu\text{g/ml}$) after incubation (at 12 h). Data is presented as Mean \pm S.D; $p < 0.05$.

4. Conclusion

Our study was based on the successful nanoencapsulation of MTX-LSMCSNPs using the polyelectrolyte complex formation technique (PEC). The encapsulation of MTX in the LSM-CS bipolymeric matrix was affirmed by FTIR and DSC analysis along with the size validation by Zeta sizer, SEM and TEM analysis with in the nano range. Our study also concludes that the efficient activity of MTX formulation as a controlled released preparation for cancer treatment was seen by the results greater than 24 h. especially at pH 5.5 (tumor pH). As cell viability (cytotoxicity was measured using HepG2 and MCF-7 cell lines) and cell apoptosis analysis (using MCF-7 cell line) was also performed, which showed that MTX loaded LSMCSNPs have more advantages to reducing the toxic side effects of nano drugs via sustained targeted delivery by using more promising natural polymers alone or in combination with the synthetic polymers.

Declaration of Competing Interest

The authors declare that they have no known competing financial interests or personal relationships that could have appeared to influence the work reported in this paper.

References

- Afshari, M., Derakhshandeh, K., Hosseinzadeh, L., 2014. Characterisation, cytotoxicity and apoptosis studies of methotrexate-loaded PLGA and PLGA-PEG nanoparticles. *J. Microencapsul.* 3, 239–245.
- Ahyat, N.M., Mohamad, F., Ahmad, A., et al., 2017. Chitin and chitosan extraction from *Portunus pelagicus*. 21, 770–777.
- Ali, S.W., Rajendran, S., Joshi, M., 2011. Synthesis and characterization of chitosan and silver loaded chitosan nanoparticles for bioactive polyester. *Carbohydr. Polym.* 83, 438–446.
- Aluigi, A., Ballestri, M., Guerrini, A., et al., 2018a. Organic solvent-free preparation of keratin nanoparticles as doxorubicin carriers for antitumour activity. *Mater. Sci. Eng. C* 90, 476–484.
- Aluigi, A., Ballestri, M., Guerrini, A., et al., 2018. Organic solvent-free preparation of keratin nanoparticles as doxorubicin carriers for antitumour activity. 90 476-484.
- Antoniraj, M.G., Leena, M.M., Moses, J., et al., 2020. Cross-linked chitosan microparticles preparation by modified three fluid nozzle spray drying approach. *Int. J. Biol. Macromol.* 147, 1268–1277.
- Athukorala, Y., Mazza, G., Oomah, B.D., et al., 2009. Extraction, purification and characterization of wax from flax (*Linum usitatissimum*) straw. *Eur. J. Lipid Sci. Technol.* 111, 705–714.
- Bashir, S., Aamir, M., Sarfaraz, R.M., et al., 2021. Fabrication, characterization and *in vitro* release kinetics of tofacitinib-encapsulated polymeric nanoparticles: a promising implication in the treatment of rheumatoid arthritis. 70 449-458.

- Bhattacharjee, S., 2016. DLS and zeta potential—what they are and what they are not? *J. Control. Release* 235, 337–351.
- Bhattacharya, S., 2020. Fabrication and characterization of chitosan-based polymeric nanoparticles of Imatinib for colorectal cancer targeting application. *Int. J. Biol. Macromol.* 151, 104–115.
- Boni, F.I., Almeida, A., Lechanteur, A., et al., 2018. Mucoadhesive nanostructured polyelectrolytes complexes modulate the intestinal permeability of methotrexate. *Eur. J. Pharm. Sci.* 111, 73–82.
- Bravo, S.A., Lamas, M.C., Salomón, C., 2002. In-vitro studies of diclofenac sodium controlled-release from biopolymeric hydrophilic matrices. *J. Pharm. Pharm. Sci.* 5, 213–219.
- Chaudhari, R., Patel, P., Meghani, N., et al., 2021. Fabrication of methotrexate-loaded gold nanoconjugates and its enhanced anticancer activity in breast cancer. 11 1-13.
- Chaudhari, R., Patel, P., Meghani, N., et al., 2021a. Fabrication of methotrexate-loaded gold nanoconjugates and its enhanced anticancer activity in breast cancer. 3 *Biotech* 11, 1–13.
- Chen, S., Zhu, J., Cheng, J., 2007. Preparation and in vitro evaluation of a novel combined multiparticulate delayed-onset sustained-release formulation of diltiazem hydrochloride. *Die Pharmazie-An Int. J. Pharm. Sci.* 62, 907–913.
- Chickpetty, S.M., Raga, B.V., 2013. Formulation, in vitro drug release and in vivo human X-ray investigation of polysaccharide based drug delivery systems for targeting 5-fluorouracil to the colon. *Brazilian J. Pharm. Sci.* 49, 263–273.
- Chiesa, E., Dorati, R., Pisani, S., et al., 2018. The microfluidic technique and the manufacturing of polysaccharide nanoparticles. *Pharmaceutics* 10, 267.
- Ciro, Y., Rojas, J., Alhaji, M.J., et al., 2020. Production and characterization of chitosan–polyanion nanoparticles by polyelectrolyte complexation assisted by high-intensity sonication for the modified release of methotrexate. *Pharmaceutics* 13, 11.
- Danaei, M., Dehghankhold, M., Atefi, S., et al., 2018. Impact of particle size and polydispersity index on the clinical applications of lipid nanocarrier systems. *Pharmaceutics* 10, 57.
- Dantas, I.L., Bastos, K.T.S., Machado, M., et al., 2018. Influence of stearic acid and beeswax as solid lipid matrix of lipid nanoparticles containing tacrolimus. *J. Therm. Anal. Calorim.* 132, 1557–1566.
- Dash, M., Chiellini, F., Ottenbrite, R.M., et al., 2011. Chitosan—A versatile semi-synthetic polymer in biomedical applications. *Prog. Polym. Sci.* 36, 981–1014.
- De Jong, W.H., Borm, P., 2008. Drug delivery and nanoparticles: applications and hazards. *Int. J. Nanomed.* 3, 133.
- Dey, S.C., Al-Amin, M., Rashid, T.U., et al., 2016. Preparation, characterization and performance evaluation of chitosan as an adsorbent for remazol red. 2, 52–62.
- Elleuch, M., Bedigian, D., Roiseux, O., et al., 2011. Dietary fibre and fibre-rich by-products of food processing: Characterisation, technological functionality and commercial applications: a review. 124, 411–421.
- Fini, A., Cavallari, C., Ceschel, G., et al., 2010. Bimodal release of olanzapine from lipid microspheres. 99, 4251–4260.
- Freitas, M., Marchetti, J., 2005. Nimesulide PLA microspheres as a potential sustained release system for the treatment of inflammatory diseases. *Int. J. Pharm.* 295, 201–211.
- Gao, C., Wang, M., Zhu, P., et al., 2021. Preparation, characterization and in vitro antitumor activity evaluation of hyaluronic acid-alendronate-methotrexate nanoparticles. *Int. J. Biol. Macromol.* 166, 71–79.
- Ghumman, S.A., Noreen, S., Tul Muntaha, S., 2020. Linum usitatisimum seed mucilage-alginate mucoadhesive microspheres of metformin HCl: fabrication, characterization and evaluation. *Int. J. Biol. Macromol.* 155, 358–368.
- Gooneh-Farahani, S., Naghib, S.M., Naimi-Jamal, M.R.J.F., et al., 2020. A novel and inexpensive method based on modified ionic gelation for pH-responsive controlled drug release of homogeneously distributed chitosan nanoparticles with a high encapsulation efficiency. 21 1917-1926.
- Grassi, M., Grassi, G., 2005. Mathematical modelling and controlled drug delivery: matrix systems. *Curr. Drug Delivery* 2, 97–116.
- Haseeb, M.T., Hussain, M.A., Abbas, K., et al., 2017. Linseed hydrogel-mediated green synthesis of silver nanoparticles for antimicrobial and wound-dressing applications. 12 2845.
- Haseeb, M.T., Hussain, M.A., Yuk, S.H., et al., 2016. Polysaccharides based superabsorbent hydrogel from Linseed: Dynamic swelling, stimuli responsive on-off switching and drug release. *Carbohydr. Polym.* 136, 750–756.
- Hashad, R.A., Ishak, R.A., Geneidi, A.S., et al., 2016. Methotrexate loading in chitosan nanoparticles at a novel pH: Response surface modeling, optimization and characterization. *Int. J. Biol. Macromol.* 91, 630–639.
- Higuchi, T., 1963. Mechanism of sustained-action medication. Theoretical analysis of rate of release of solid drugs dispersed in solid matrices. *J. Pharm. Sci.* 52, 1145–1149.
- Hintz, R.J., Johnson, K.C., 1989. The effect of particle size distribution on dissolution rate and oral absorption. *Int. J. Pharm.* 51, 9–17.
- Jia, M., Li, Y., Yang, X., et al., 2014. Development of both methotrexate and mitomycin C loaded PEGylated chitosan nanoparticles for targeted drug codelivery and synergistic anticancer effect. *ACS Appl. Mater. Interfaces* 6, 11413–11423.
- Kou, Z., Dou, D., Mo, H., et al., 2020. Preparation and application of a polymer with pH/temperature-responsive targeting. 165 995-1001.
- Kurra, P., Narra, K., Puttugunta, S.B., et al., 2019. Development and optimization of sustained release mucoadhesive composite beads for colon targeting. *Int. J. Biol. Macromol.* 139, 320–331.
- Kwak, S.-Y., Lew, T.T.S., Sweeney, C.J., et al., 2019. Chloroplast-selective gene delivery and expression in planta using chitosan-complexed single-walled carbon nanotube carriers. 14, 447–455.
- Li, N., Wang, C., Georgiev, M.I., et al., 2021. Advances in dietary polysaccharides as anticancer agents: Structure-activity relationship. *Trends Food Sci. Technol.* 111, 360–377.
- Libo, Y., Reza, F., 1996. Kinetic modeling on drug release from controlled drug delivery system. *Acta Pol Pharm* 85, 170.
- Lima, A.C., Sher, P., Mano, J.F., 2012. Production methodologies of polymeric and hydrogel particles for drug delivery applications. *Expert Opin. Drug Deliv.* 9, 231–248.
- Liu, D., Jiang, S., Shen, H., et al., 2011. Diclofenac sodium-loaded solid lipid nanoparticles prepared by emulsion/solvent evaporation method. *J. Nanopart. Res.* 13, 2375–2386.
- Liu, J., Shim, Y.Y., Tse, T.J., et al., 2018. Flaxseed gum a versatile natural hydrocolloid for food and non-food applications. *Trends Food Sci. Technol.* 75, 146–157.
- Malviya, R., Raj, S., Fuloria, S., et al., 2021. Evaluation of antitumor efficacy of chitosan-tamarind gum polysaccharide polyelectrolyte complex stabilized nanoparticles of simvastatin. 16 2533.
- Mauludin, R., Müller, R.H., Keck, C.M., 2009. Development of an oral rutin nanocrystal formulation. *Int. J. Pharm.* 370, 202–209.
- Mircioiu, C., Voicu, V., Anuta, V., et al., 2019. Mathematical modeling of release kinetics from supramolecular drug delivery systems. 11, 140.
- Moghaddas, S.M.T.H., Elahi, B., Darroudi, M., et al., 2019. Green synthesis of hexagonal-shaped zinc oxide nanosheets using mucilage from flaxseed for removal of methylene blue from aqueous solution. *J. Mol. Liq.* 296, 111834.
- Najafipour, A., Gharieh, A., Fassih, A., et al., 2020. MTX-loaded dual thermoresponsive and pH-responsive magnetic hydrogel nanocomposite particles for combined controlled drug delivery and hyperthermia therapy of cancer. *Mol. Pharm.* 18, 275–284.
- Naran, R., Chen, G., Carpita, N.C., 2008. Novel Rhamnogalacturonan I and Arabinoxylan Polysaccharides of Flax Seed Mucilage. 148, 132-141.
- Nasrabadi, M.N., Goli, S.A.H., Doost, A.S., et al., 2019. Plant based Pickering stabilization of emulsions using soluble flaxseed protein and mucilage nano-assemblies. 563, 170-182.

- Noreen, S., Hasan, S., Ghumman, S.A., et al, 2022. pH Responsive Abelmoschus esculentus Mucilage and Administration of Methotrexate: In-Vitro Antitumor and In-Vivo Toxicity Evaluation. *Int. J. Mol. Sci.* 23, 2725.
- Nosrati, H., Salehiabar, M., Davaran, S., et al., 2018. Methotrexate-conjugated L-lysine coated iron oxide magnetic nanoparticles for inhibition of MCF-7 breast cancer cells. 44, 886-894.
- Ong, S.G.M., Ming, L.C., Lee, K.S., et al., 2016. Influence of the encapsulation efficiency and size of liposome on the oral bioavailability of griseofulvin-loaded liposomes. 8 25.
- Patwekar, S., Potulwar, A., Pedewad, S., et al., 2016. Review on polyelectrolyte complex as novel approach for drug delivery system. 5, 98-109.
- Potaś, J., Szymańska, E., Winnicka, K.J.E.P.J., 2020. Challenges in developing of chitosan-based polyelectrolyte complexes as a platform for mucosal and skin drug delivery. 140 110020.
- Priya, K., Vijayakumar, M., Janani, B., 2020. Chitosan-mediated synthesis of biogenic silver nanoparticles (AgNPs), nanoparticle characterisation and in vitro assessment of anticancer activity in human hepatocellular carcinoma HepG2 cells. *Int. J. Biol. Macromol.* 149, 844-852.
- Qian, K., Cui, S., Wu, Y., et al, 2012. Flaxseed gum from flaxseed hulls: Extraction, fractionation, and characterization. *Food Hydrocoll.* 28, 275-283.
- Rahimi, M., Shojaei, S., Safa, K.D., et al, 2017. Biocompatible magnetic tris (2-aminoethyl) amine functionalized nanocrystalline cellulose as a novel nanocarrier for anticancer drug delivery of methotrexate. *New J. Chem.* 41, 2160-2168.
- Rajabi, H., Jafari, S.M., Rajabzadeh, G., et al., 2019. Chitosan-gum Arabic complex nanocarriers for encapsulation of saffron bioactive components. 578, 123644.
- Ramteke, K., Dighe, P., Kharat, A., et al., 2014. Mathematical models of drug dissolution: a review. 3, 388-396.
- Ray, S., Joy, M., Sa, B., et al, 2015. pH dependent chemical stability and release of methotrexate from a novel nanoceramic carrier. *RSC Adv.* 5, 39482-39494.
- Rocha, M. S., L. C. Rocha, M. B. da Silva Feijó, et al., 2021. Effect of pH on the flaxseed (*Linum usitatissimum* L. seed) mucilage extraction process. 43, e50457-e50457.
- Sahu, B.P., Das, M.K., 2014. Nanosuspension for enhancement of oral bioavailability of felodipine. *Appl. Nanosci.* 4, 189-197.
- Salem, D.S., Shouman, S.A., Badr, Y., 2019. Laser-triggered release of drug encapsulated in chitosan nanoparticles for therapy of hepatocellular carcinoma. *SPIE, Colloidal Nanoparticles for Biomedical Applications XIV*, p. 108920Z.
- Shafiq, A., Madni, A., Khan, S., et al, 2022. Core-shell Pluronic F127/chitosan based nanoparticles for effective delivery of methotrexate in the management of rheumatoid arthritis. *Int. J. Biol. Macromol.* 213, 465-477.
- Sheikh, F.A., Hussain, M.A., Ashraf, M.U., et al, 2020. Linseed hydrogel based floating drug delivery system for fluoroquinolone antibiotics: Design, in vitro drug release and in vivo real-time floating detection. *Saudi Pharm. J.* 28, 538-549.
- Sindhu, R., Binod, P., Pandey, A., 2015. Chapter 17 - Microbial Poly-3-Hydroxybutyrate and Related Copolymers. In: Pandey, A., Höfer, R., Taherzadeh, M. (Eds.), *Industrial Biorefineries & White Biotechnology*. Elsevier, Amsterdam, pp. 575-605.
- Souza, T.G., Ciminelli, V.S., Mohalle, N.D.S., 2016. A comparison of TEM and DLS methods to characterize size distribution of ceramic nanoparticles. *J. Phys.: Conf. Ser.*, IOP Publishing. 733, 012039.
- Taheri, A., Atyabi, F., Salman Nouri, F., et al., 2011. Nanoparticles of conjugated methotrexate-human serum albumin: preparation and cytotoxicity evaluations. 2011.
- Takano, R., Furumoto, K., Shiraki, K., et al, 2008. Rate-limiting steps of oral absorption for poorly water-soluble drugs in dogs; prediction from a miniscale dissolution test and a physiologically-based computer simulation. *Pharm. Res.* 25, 2334-2344.
- Toomari, Y., Namazi, H., 2016. Synthesis of supramolecular biodendrimeric β -CD-(spacer- β -CD) 21 via click reaction and evaluation of its application as anticancer drug delivery agent. *Int. J. Polym. Mater. Polym. Biomater.* 65, 487-496.
- Weng, J., Tong, H.H., Chow, S.F.J.P., 2020. In vitro release study of the polymeric drug nanoparticles: development and validation of a novel method. 12, 732.
- Yousefpour, P., Atyabi, F., Dinarvand, R., 2011. Preparation and comparison of chitosan nanoparticles with different degrees of glutathione thiolation. *DARU: J. Fac. Pharm. Tehr. Univ. Med. Sci.* 19, 367-375.
- Zhao, Y., Guo, Y., Li, R., et al, 2016. Methotrexate nanoparticles prepared with codendrimer from polyamidoamine (PAMAM) and oligoethylene glycols (OEG) dendrons: Antitumor efficacy in vitro and in vivo. *Sci. Rep.* 6, 1-11.